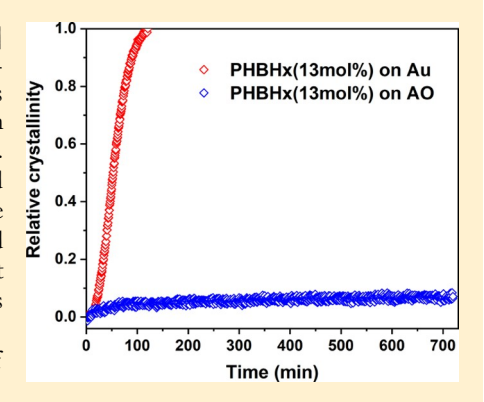


Crystallization Retardation of Ultrathin Films of Poly(R)-3hydroxybutyrate] and a Random Copolymer Poly[(R)-3hydroxybutyrate-co-(R)-3-hydroxyhexanoate] on an Aluminum Oxide Surface

Changhao Liu, ** Isao Noda, ** D. Bruce Chase, ** Yuying Zhang, ** Jing Qu, ** Meng Jia, ** Chaoying Ni, ** and John F. Rabolt*, to

ABSTRACT: Ultrathin films of biodegradable poly[(R)-3-hydroxybutyrate](PHB) and its random copolymer poly[(R)-3-hydroxybutyrate-co-(R)-3-hydroxyhexanoatel (PHBHx) were prepared by spin-coating onto aluminum substrates with a naturally oxidized aluminum oxide (AO) surface layer or, alternatively, on gold substrates. The opposite surface of the film was in contact with ambient air. Isothermal crystallization kinetics of these films at room temperature were studied using infrared reflection absorption spectroscopy. The overall crystallization rate for all the polymers when crystallizing on AO is significantly retarded compared with the same polymer crystallizing on gold. It was found that the retardation effect was not due to a confinement effect. The crystallization retardation effect was especially enhanced for PHBHx with a higher (R)-3-hydroxyhexanoate content. Avrami analysis showed that the crystallization rate constant k (min⁻¹) for all of the polymers on AO is approximately 3 to 4 orders of magnitude less than that found for the same polymer on gold. Grazing incident wide-angle X-ray diffraction



showed that polymers on gold have both flat-on and edge-on crystallite orientations, whereas polymers on AO have a dominating edge-on crystallite orientation. Infrared studies on a quasi-monolayer film revealed no detectable H-bonding between PHB/PHBHx and the AO surface. The crystallization retardation mechanism was explained as being a sum of the dipole – dipole interactions of – C D of PHB or PHBHx and the – O – Al – O – groups of AO coupled with the rigid disordered amorphous nature of the AO surface.

INTRODUCTION

Poly[(R)-3-hydroxybutyrate] (PHB) and its random copolymer poly[(R)-3-hydroxybutyrate-co-(R)-3-hydroxyhexanoate](PHBHx) are bio-based and biodegradable aliphatic polyesters that can be produced by bacterial fermentation.¹⁻⁴ PHB and PHBHx have gained substantial interest in both the academic and industrial research communities as environmentally friendly polymers. PHB and PHBHx serve as energy and carbon storage materials when synthesized in the cells of microorganisms. The PHB homopolymer suffers from both a high melting temperature, which is close to the thermal degradation temperature, and brittleness because of excessively high crystallinity.3 PHBHx, now commercialized as Nodax by Danimer Scientific (Bainbridge, GA), can be biosynthesized by randomly incorporating a noncrystalline comonomer unit (R)-3-hydroxyhexanoate (3HHx), giving rise to a lower melting temperature and reduction in crystallinity, leading to a tougher material. Because of desired material properties including mechanical properties comparable to polypropylene, good gas

barrier properties, and good biocompatibility, many uses of PHB and PHBHx are being explored in plastics, the packaging industry, and medical applications such as tissue engineering scaffolds.5

Extensive studies have shown that both PHB and PHBHx exhibit intriguing crystallization profiles. Two crystal polymorphs have been identified so far: the alpha crystal form with an orthorhombic unit cell (space group: $P2_12_12_1$, a = 5.76 Å, b= 13.20 Å, and c = 5.96 Å)^{6,7} and the beta form containing a planar zigzag chain conformation, typically found as a metastable ordered phase.8-10 Formation of alpha crystals has been found to be driven by an unusually weak but cooperative H-bonding formed between the hydrogen of methyl group from one helix and the oxygen of carbonyl group from an adjacent helix in the crystal.¹¹⁻¹⁴ This unusual H-

Received: June 14, 2019 September 11, 2019 Published: September 24, 2019



[†]Department of Materials Science and Engineering, §Advanced Materials Characterization Lab, and [∥]Department of Chemistry, University of Delaware, Newark 19716, Delaware, United States

Danimer Scientific, Bainbridge 39817, Georgia, United States

[🐣] Supporting Information

bonding network appears to enable the formation of a thermodynamically stable crystal structure even with the substantial presence of noncrystallizing comonomer units. The beta form has additional promising material properties and functionality, such as a higher tensile strength and significant piezoelectricity. Thus, exploring technical methods to retard or inhibit the alpha crystallization of PHB has practical significance. Inhibiting the alpha crystallization can make the polymer easier to process with improved material toughness. Slowing down the alpha crystallization also benefits

the production of the beta form. Making beta form is a technical challenge because of the unusually rapid formation of alpha crystals. Therefore, if the amorphous state can be maintained below the melting temperature, the operating time window to process the polymer (such as during film stretching) to induce beta-form crystals will be broadened. 15,16

Protocols to produce amorphous PHB in general fall into two categories. The first involves creating a spatially confined environment to inhibit PHB from crystallizing by mimicking the native PHB amorphous granules found in cells. ¹⁸ In vivo, PHB and PHBHx maintain an amorphous granular state, ¹⁹ which is believed to be driven by a spatial confinement and

isolation effect in the cell. For example, PHB nanorods fabricated from a porous three-dimensional anodized aluminum oxide (AAO) scaffold were found not to crystallize when the pore size is small.²⁰ In this study, the inhibition effect was also found to correlate with the degree of curvature of the confinement pore. In another example, a 16 nm PHB ultrathin

film sandwiched between a Si wafer and an amorphous polymer layer was found not to be able to crystallize, existing as an amorphous layer irrespective of crystallization temperatures. ²¹ Napolitano and Wübbenhorst also reported that PHB ultrathin films sandwiched between two aluminum plates were also found not to crystallize. ²² However, in these systems, once the confinement constraints were released, the polymer then started to crystallize. Alternatively, another approach to inhibit PHB crystallization is through a surface-induced crystallization inhibition by utilizing substrates with surface chemistries capable of interacting with PHB to retard or inhibit crystallization. This method has more practical relevance because it has the potential to inhibit or retard crystallization in

a less constrained environment. For example, Capitant al. found that the crystallization of PHB nanofilms was inhibited when one side of the film was in contact with glass while the other side was exposed to the ambient environment and free from such contact.²³ In this system, the confinement effect is much less compared to the sandwiched structure. This surface-

induced inhibition effect may also provide access to the development of nanocomposites by blending PHB/PHBHx with nanoparticles having similar surface properties. Therefore, it is important to explore other substrates with the potential to inhibit PHB crystallization.

In Napolitano's work,²² reasons for the inhibition effect remain an open question. It is it due to a size effect or the intrinsic aluminum oxide (AO) surface chemistry effect?". In this paper, we will demonstrate that the crystallization retardation and inhibition of PHB and PHBHx on a flat AO surface still exist even for thin films with one surface exposed to air. To our knowledge, this is the first demonstration that an AO surface itself, without confinement, can retard crystallization of PHB and PHBHx.

In the current study, thin films of both PHB and PHBHx were spin-coated on flat aluminum substrates (with a native

oxide layer) and also on gold substrates. The gold substrate was used as the reference surface for comparison. The real-time crystallization process was recorded using infrared reflection—absorption spectroscopy (IRRAS). The kinetic data for all the samples were evaluated using Avrami analysis. Two-dimensional grazing incident wide-angle X-ray diffraction (GI-WAXD) was used to examine the crystal orientation in the films. A mechanism of AO-induced crystallization inhibition of PHB and PHBHx is proposed based on the Avrami analysis and the surface structure of AO.

EXPERIMENTAL SECTION

Materials. PHB was purchased from Sigma-Aldrich (St. Louis, MO, USA) while PHBHx with different 3HHx concentrations and atactic PHB (aPHB) were provided by the Procter & Gamble Company (Cincinnati, OH, USA). The molecular weight (weight-averaged) for PHBHx(5.8 mol %), PHBHx(9.4 mol %), and PHBHx(13 mol %) is 461 387, 454 501, and 840 000 g/mol, respectively. Chloroform was purchased from Fisher Scientific. Methylene iodide (MI) used for contact angle measurements was purchased from Sigma-Aldrich. All the as-received polymers were purified by a two-step standard purification method to remove polar and nonpolar impurities. 11 Other chemicals were used as received.

Gold-coated glass substrates were purchased from Platypus Technologies LLC while aluminum-coated glass substrates were purchased from Deposition Research Lab Inc. Both the substrates were prepared by physical vapor deposition and the deposition layers were approximately 100 nm thick. After deposition, the aluminum-coated substrates were allowed to naturally oxidize by being exposed to ambient air at room temperature (around 23 °C). To remove physically adsorbed water, both gold and aluminum substrates were purged under nitrogen for 30 min before spin-coating. The roughness profiles in root mean square for the two substrates were determined using a Dimension 3100 atomic force microscope, were 1.27 and 1.52 nm for gold and aluminum, respectively (see Supporting Information S1).

Thin-Film Preparation. A solution of 0.5 wt % polymer in chloroform was used for spin-coating. A 0.5 mL loading of polymer solution was used. A 1300 rpm/s acceleration rate was applied, and the spin coater was operated at 4000 rpm for 3 min. These spincoating conditions resulted in a thin film of approximately 40 nm thickness. The film thickness was determined using X-ray reflectometry (see Supporting Information S2). For melt crystallization, the as-spin-coated film was first placed on a preheated hot plate equipped with a ceramic top surface. The exact melting time applied for each sample was dependent on the specific polymer and substrate. The heating profile for each sample is listed in Supporting Information S3. Once melting was complete, the sample was immediately placed in contact with a 5 °C copper surface to cool it down to room temperature. The sample was then rapidly transferred into the infrared spectrometer chamber for recording of its spectrum. The interval between cooling and recording the first spectrum was 2

Infrared Reflection—Absorption Spectroscopy. IRRAS measurements were conducted using a Thermo Nicolet 670 Nexus FT-IR spectrometer with a DTGS detector. A specular reflectance accessory (PIKE Tech. 80Spec) was used with a fixed incident angle of 80°. Gold and aluminum mirrors at 80° incident angle have the same absorption factor, as shown by Greenler's paper. Each spectrum was collected by averaging 32 scans with a 4 cm⁻¹ resolution from 600 to 4000 cm⁻¹. The as-collected raw spectra were baseline-corrected using the Essential FTIR software.

Grazing Incident Wide-Angle X-ray Diffraction. An Xeuss 2.0 X-ray diffractometer equipped with a two-dimensional X-ray detector was used to examine the in-plane and out-of-plane crystallite orientation profiles. The instrument was operated at a current of 0.6 mA and voltage of 50 kV. Cu Kα radiation with an X-ray wavelength of 0.154 nm was used. The grazing angle used was 0.2°,

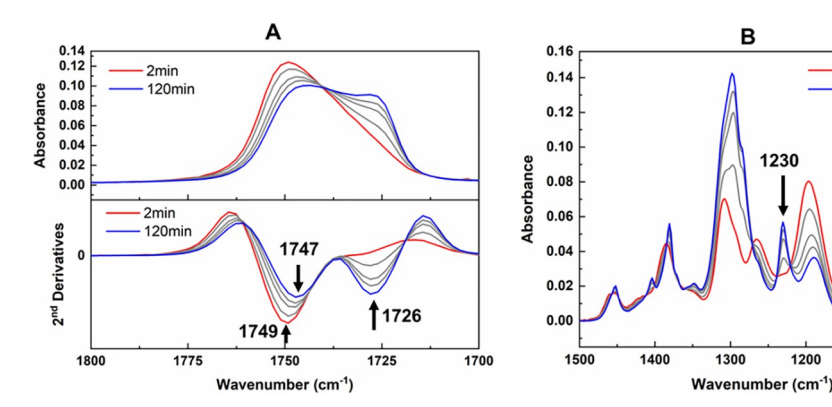


Figure 1. IRRAS spectra and second-derivative spectra of carbonyl stretching region (A), and backbone region (B) for PHB crystallization on gold at room temperature.

which is approximately 1.2 times the critical angle at these experimental conditions and ensures that the X-ray beam penetrates the entire sample. Samples for GIWAXD measurements were investigated after a 5-day room-temperature crystallization. GIWAXD experiments were conducted at room temperature.

X-ray Photoelectron Spectroscopy. The X-ray photoelectron spectroscopy (XPS) spectra were collected on a Thermo Scientific K-Alpha XPS instrument with an Al K α X-ray source at an energy of 1486.6 eV at a base pressure below 5 × 10⁻⁸ Torr. The takeoff angle was 90° with respect to the analyzer, ensuring maximum collection efficiency. The survey spectrum was collected with an energy range of 0–1200 eV (a survey spectrum is shown in Supporting Information S4). The high-resolution spectra for C 1s, O 1s, and Al 2p were collected with the pass energy of 20 eV. The data analysis was performed with CasaXPS (version 2.3.16) software. All peak positions and relative sensitivity factors were calibrated to the C 1s peak at 285 eV.²⁵

Transmission Electron Microscopy. To examine the structure of the aluminum substrate surface, a replica of the aluminum substrate cross section was prepared using a focused ion beam lift-out approach (Zeiss Auriga 60 dual beam scanning electron microscopy). The outmost layer was protected by sputtering a gold protection layer to prevent potential beam damage. A Talos F200C TEM operated at a voltage of 200 kV was used for recording the high-resolution image of the aluminum/AO interfacial region.

RESULTS AND DISCUSSION

Typical IRRAS Spectra during Room-Temperature Crystallization. Measuring crystallization kinetic profiles is traditionally carried out using differential scanning calorimetry (DSC). However, this technique is typically reserved for bulk samples. For ultrathin films attached to reflective substrates, IRRAS serves as a powerful tool for the study of crystallization kinetics. Using infrared spectroscopy to quantitatively study transformation kinetics has been reported previously, where it has been shown that the IR measurement-derived kinetics matched well with the DSC measurements. ^{26,27} In this study, in order to demonstrate the crystallization retardation of PHB and PHBHx on an aluminum substrate, a gold substrate was used as the reference substrate because of the inert nature of gold to polyesters.

Preliminary results showed that the typical changing trend of spectra for all the samples only differs in the changing rate of IR peak intensity. Hence, we first examine the typical IR spectra during room-temperature crystallization using PHB/gold as an example. For PHB crystallization on gold, we found that within 120 min, crystallization was complete. We, therefore, selected five IRRAS spectra taken at 2, 5, 10, 15,

and 120 min, respectively, to show spectral changes, as detailed in Figure 1.

1100

2min

In the carbonyl stretching region (Figure 1A), at the very beginning, only a peak at 1749 cm⁻¹ appears, which is attributed to the carbonyl from the amorphous material. As crystallization proceeds, a peak located at 1726 cm⁻¹ grows, which is assigned to the carbonyl stretch in alpha crystals. 13 In addition, with crystallization, the amorphous peak maximum at 1749 cm⁻¹ shifted to approximately 1747 cm⁻¹, possibly indicating that the local environment of an amorphous carbonyl changes from a less restricted environment to a more restricted environment. It is most likely due to the amorphous carbonyls located near the thin-film-free surface prior to crystallization, which have been transformed into interlamellar amorphous carbonyls after crystallization. In the interlamellar region, a more restricted local environment is expected. The higher-wavenumber amorphous carbonyl in PHB and PHBHx systems has also been reported in other studies recently.^{28,29} The alpha crystallization can also be seen by examining the backbone region (Figure 1B). The peak located at 1230 cm⁻¹ can be assigned to -C-O-Cstretching in the crystalline region.³⁰ The bands at 1230 and 1726 cm⁻¹ were found to increase simultaneously. In the current crystallization kinetics study, we will use the wellisolated band at 1230 cm⁻¹ to evaluate the crystallinity changes during crystallization. The relative crystallinity at any given time can be described by

$$X_t = \frac{I_t - I_0}{I_\infty - I_0}$$

where X_t is the relative crystallinity at time t, and I_0 , I_t , and I_∞ are the 1230 cm⁻¹ peak intensities at time zero, time t, and time infinity, respectively. In this experiment, the value used for I_∞ was from the sample after 5-day crystallization at room temperature. This is because the major development of the overall crystallinity in polymer crystallization is mostly derived from primary crystallization. We found that, for our samples, the primary crystallization was mostly complete within 5 days, even for PHBHx(13 mol %) on Al, which has the lowest crystallization rate.

Time-Dependent Relative Crystallinity of PHB and PHBHx on Gold and Aluminum Substrates. We first examine the time-dependent crystallinity profiles on a gold substrate as a function of 3HHx content, and these are shown in Figure 2. As one can see, all transformations show classic "S"-shaped curves. The "S"-shaped curve is typically divided

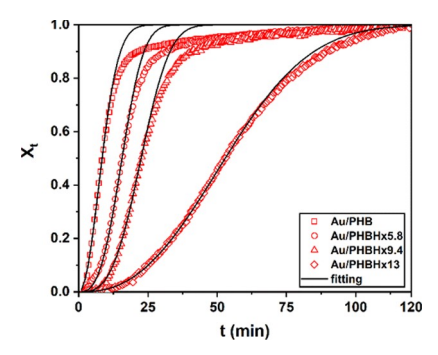


Figure 2. PHB and PHBHx time-dependent crystallinity profiles on gold as a function of 3HHx. Red profiles are experimental data points. Black profiles are fittings based on Avrami analysis.

into three crystallization regions (see Supporting Information S5): induction period, primary crystallization period, and secondary crystallization period. A couple of interesting kinetic features can be identified. First, crystallization occurs relatively fast for all the polymers on gold. Even for PHBHx (13 mol % 3HHx), after 120 min, the primary crystallization was complete, and the sample was well into the secondary crystallization period. This fast crystallization rate implies that the polymer has enough chain segmental mobility in this asymmetric ultrathin film with film/air interface. We note that the very first spectrum for PHB/Au sample already showed a small peak on 1230 cm⁻¹ (see Supporting Information S6), indicating that crystallization probably already occurred during cooling. Second, the overall crystallization rate decreases with increasing 3HHx content. This is expected because a higher

3HHx comonomer content makes nucleation and growth more difficult. Chain segment mobility should be reduced because of the steric effect of 3HHx, a relatively bulky medium-length-chain side group.

The time-dependent relative crystallinity profiles of different polymers on aluminum substrates are shown in Figure 3. The crystallinity profile on gold for each polymer was included for comparison. It can be seen that for all polymers, crystallization on an aluminum substrate is significantly slower than that for a gold substrate. Especially intriguing is the case of PHBHx (13 mol %) (Figure 3D), where the induction period can last as long as 12 h. We also found that 48 h were needed for PHBHx (13 mol %) to reach a crystallinity of 50%.

Avrami Analysis of Crystallization Kinetics. Previous results showed that on an aluminum substrate, all the polymers exhibit crystallization retardation. In order to further elucidate the effect of an aluminum substrate on the crystallization mechanisms and control factors, we attempted to fit the kinetic data into a classic Avrami equation. The validation of applying Avrami equation to two-dimensional ultrathin films has been demonstrated in previous work by others.31-33 The Avrami equation can be expressed as³⁴ $X_t = 1 - \exp(-kt^n)$, or in the form of double logarithm, $\ln(-\ln(1 - X_t)) = \ln k + n \ln t$, where X_t is the relative crystallinity as mentioned before, k(min⁻¹) is the overall crystallization rate constant accounting for both nucleation and growth process, and n is the Avrami index, describing a crystallization mechanism. The overall Avrami index n can be further decomposed and described by n $= n_1 + cn_2$, where n_1 is the nucleation index, n_2 is the growth dimensionality, and c is the growth index.³⁵ In our case, the growth dimension is 2 for all the samples, so $n_2 = 2$ because all

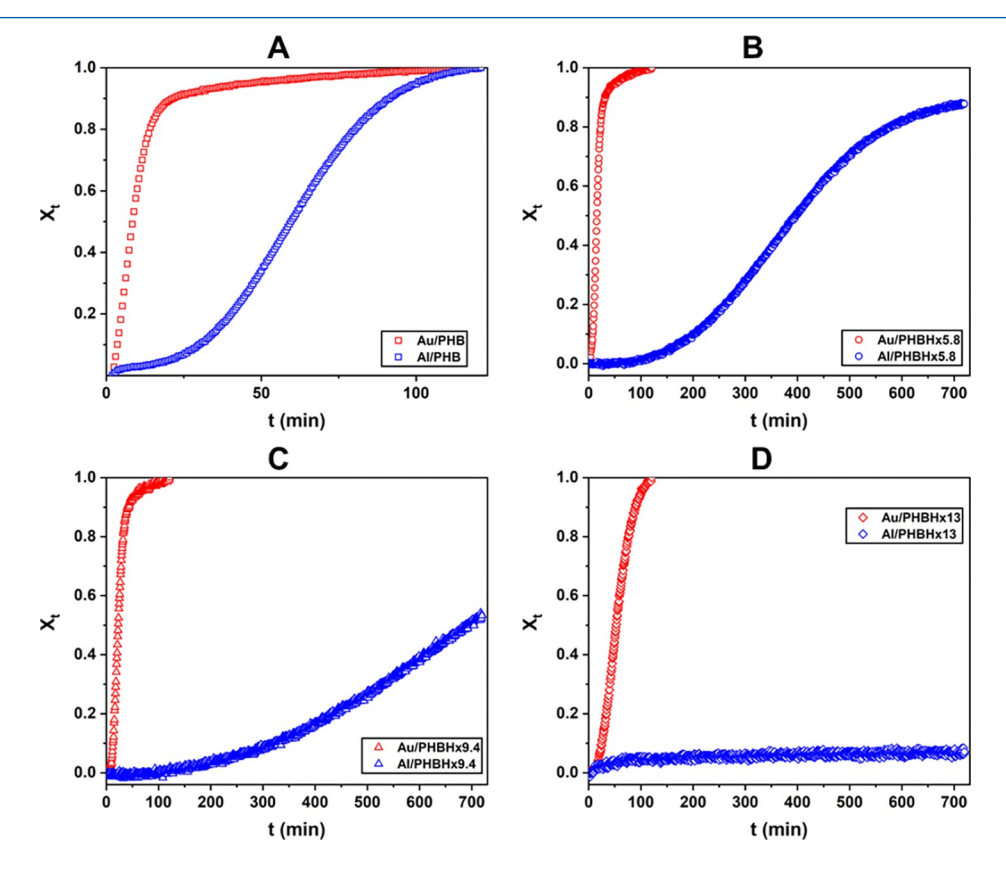


Figure 3. Relative crystallinity profile of different polymers on gold and aluminum substrates. A: PHB; B: PHBHx (5.8 mol %); C: PHBHx (9.4 mol %); and D: PHBHx (13 mol %). Red curve: gold. Blue curve: aluminum.

the samples are two-dimensional ultrathin films. For a complete instantaneous nucleation, $n_1 = 0$, whereas for a complete sporadic nucleation, $n_1 = 1$. Nonintegral n_1 was also found in many cases because of the processes between instantaneous and sporadic nucleation. The growth index c describes whether the crystallization mechanism is interface-controlled or diffusion-controlled. For a complete interface control, c = 1, whereas for a complete diffusion control, c = 0.5. Values between 0.5 and 1 can be interpreted as both control factors contributing to the overall growth mechanism.

In the current study, kinetic data in the crystallinity range of $15\% < X_t < 50\%$ were used for the curve fitting for all the samples. Results are shown in Figure 4. Because of an

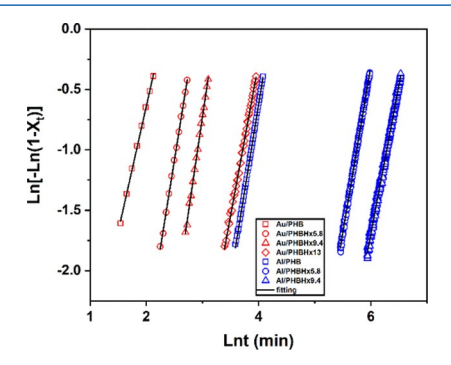


Figure 4. Avrami plot of PHB and PHBHx with varying 3HHx content on gold (red) and aluminum (blue) substrate. Black lines are the fittings.

extensively long induction period, fitting for PHBHx (13 mol %)/Al failed, so it is not included in the figure. For all the other samples, the overall Avrami index n and rate constant k can be directly extracted from the curves and they are listed in Table 1. The extracted values of n are plotted as a function of 3HHx

Table 1. Kinetic Parameters Derived from Experimental Avrami Analysis

	polymer	n	$k (\text{min}^{-1})$	$t_{1/2}$ (min)
gold	PHB	2.07	8.41×10^{-3}	8
	PHBHx5.8	2.91	2.35×10^{-4}	16
	PHBHx9.4	3.16	3.71×10^{-5}	23
	PHBHx13	2.53	3.04×10^{-5}	53
aluminum	PHB	2.87	5.50×10^{-6}	60
	PHBHx5.8	2.76	4.65×10^{-8}	395
	PHBHx9.4	2.46	6.96×10^{-8}	693

content for gold and aluminum substrates, as shown in Figure 5A. We can see that as 3HHx increases, when deposited on gold, n first increases, and then decreases [for PHBHx (13 mol %)]. This indicates that when it is deposited on gold and as 3HHx increases, nucleation becomes more difficult, making n_1 increase, leading to an overall increase in n. When 3HHx increases to 13 mol %, it is highly possible that diffusion control occurs causing c to decrease and thus leading to a decrease in n.

For crystallization on an Al substrate, two facts can be concluded from Figure 5A. First, for PHB, the Avrami index n(Al) is greater than n(Au), indicating that the nucleation has become more difficult on an Al substrate. Second, n(Al) decreases with increased 3HHx content. This straightforward, decreasing trend is different than the variable trend of n(Au),

where *n*(Au) first increases and then decreases. Hypothetically, this difference occurs because diffusion control starts taking effect at 5.8 mol % 3HHx content in the Al case. Because Avrami analysis is a semiempirical method, supplementary experimental techniques such as dielectric spectroscopy may be applied in the future to reveal more details of chain dynamics of PHB/PHBHx on AO surfaces.²⁰

Now, let us examine the overall rate constant k, as shown in Table 1. We found that on gold, all the polymers show a rate constant, k, with comparable order of magnitude with respect to that found in the bulk.³⁶ This observation suggests that we have an ultrathin film system with comparable crystallization kinetics compared to the bulk. This result is most likely because the chain has enhanced mobility on the film/air interface and has a weakened mobility on the substrate surface, leading to the two effects canceling out each other, giving rise to bulk-like crystallization kinetics. Our system, thus, is very different from the confined systems, such as in an AAO porous scaffold and in two-plate sandwiched structures. 20,22 In addition, k for PHB/Au is high, equivalent to a bulk crystallization rate at 48 or 90 °C.36 This is an additional line of evidence that, for this particular sample, the nucleation starts during cooling, consistent with the previous IR observation. However, the k values for polymers on aluminum, in general, are around 3 to 4 orders of magnitude less than those found on gold. For PHBHx with high 3HHx content, k can be as low as 10^{-8} min⁻¹. The crystallization half-time, denoted as $t_{1/2}$, can be calculated from $t_{1/2} = [(\log 2)/k]^{1/n}$ (or $X_t = 1 - \exp(-kt_1^n)$. A retardation factor, hence, can be defined as $F_r = t_{1/2}[AI]/t_{1/2}[Au]$ to reflect the inhibition effect of Al on crystallization for different polymers. The plot of F_r as a function of 3HHx is shown in Figure 5B. One can clearly see that an aluminum substrate shows an increasing crystallization retardation effect for the copolymers with increased 3HHx, suggesting that at high 3HHx, the retardation effect was enhanced. This observation is consistent with our Avrami index analysis, that is, at a higher 3HHx content, the diffusion control factor dominates, and Al has a more prominent hindering effect on the diffusion process.

Mechanism Study of Crystallization Retardation. We first examine the possible interactions between PHB/PHBHx and an aluminum substrate surface. The elemental analysis of the surface of an Al substrate was performed using XPS, as shown in Figure 6. As expected, Al 2p and O 1s profiles clearly indicate the presence of AO on the surface. In addition, a weak hydroxyl peak (from peak fitting) from Al-OH was observed, indicating that a trace amount of chemically bound -OH is present on the AO surface. Previous studies have shown that ester groups in certain polymers are able to form a H-bonded interaction with surface hydroxyl groups from an AO surface.^{37,38} For instance, in the work by Brogly et al., the ester group in poly(methyl methacrylate) (PMMA) was able to H-bond with Al-OH, leading to a 10 cm⁻¹ red shift of the carbonyl peak from 1740 to 1730 cm⁻¹. Ulrent al. found that the ester group from poly(ethylene-co-butyl acrylate) (EBA) forms a H-bonded interaction with species on the AO surface, giving rise to an 8 cm⁻¹ red shift of the carbonyl peak. In the current study, however, no evidence of a red shift resulting from H-bonding was observed in all the samples. Three possible reasons are proposed for the absence of the red shift of the carbonyl stretching band for PHB and PHBHx. First, it is possible that the H-bonding interaction does not exist, or if it does, the interaction might be too subtle to be detected by the

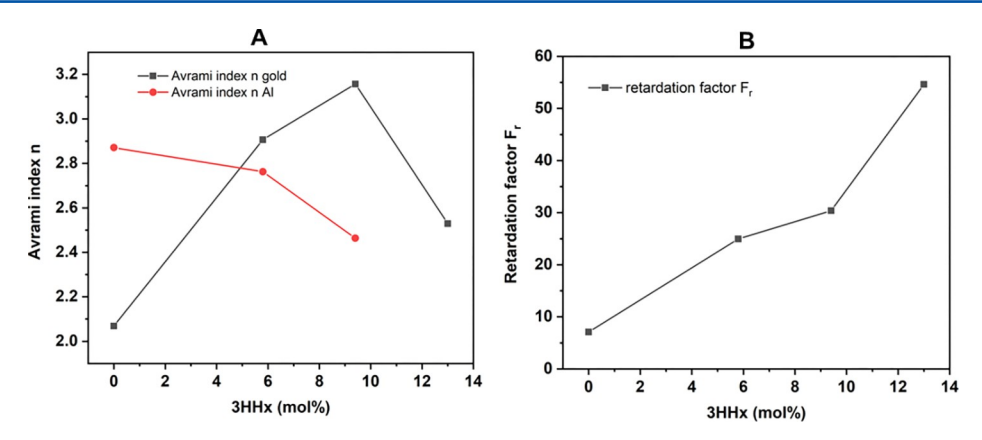


Figure 5. A: Avrami index plot against 3HHx content on gold (black) and aluminum (red) substrates. B: Plot of retardation factor F_r against 3HHx content.

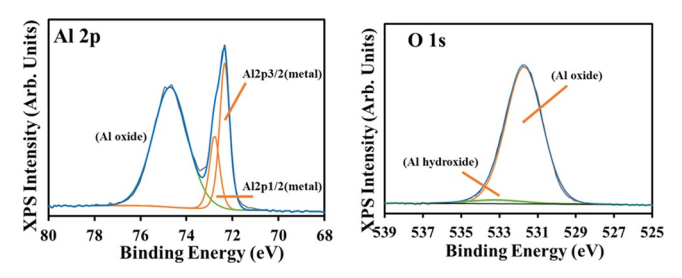


Figure 6. XPS profiles of the surface of aluminum substrate. Left: Al 2p profile. Right: O 1s profile.

IRRAS measurement. The XPS data indeed show that the −OH species on AO is very minimal. In studies by Brogly et al. and Ulrent al., the detailed chemical nature of the AO surfaces and the surface treatments used were not discussed. Thus, it is possible that the AO surfaces used in their studies have more −OH than our AO surfaces, which can lead to H-bond formation. Second, if we hypothesize that a trace amount of −OH can form H-bonds with −ŒO from PHB/PHBHx, then the interaction would be located near the 1−2 nm interfacial layer of polymer/substrate. A 40 nm film would be too thick for us to detect this potential H-bonding interaction. Third, another possible reason for the absence of a red shift could be that the new peak due to the potential H-bonding is obscured by the crystalline carbonyl peak at 1726 cm⁻¹ due to crystallization.

To eliminate the latter two possibilities, we used aPHB, which is incapable of crystallizing because of its atactic architecture, to study the interaction of polymer/substrate.

Thus, any red shift from the 1749 cm⁻¹ amorphous peak must come from the interaction between aPHB with an AO surface. In addition, to study the interaction from the actual polymer/ substrate interfacial layer, we prepared nanolayer thin films of aPHB using a 0.003 wt % aPHB in a chloroform solution. The film thickness of this nanolayer is estimated to be 1.36 nm. Detailed preparation conditions and thickness calculation can be found in Supporting Information S7. The IRRAS spectra of both aPHB nanolayer and aPHB 40 nm "thick" films are displayed in Figure 7. We see a 2 cm⁻¹ red shift from 1749 to 1747 cm⁻¹ for the aluminum substrate, but a similar peak displacement was also seen in the gold case, suggesting that this slight shift is not limited to Al substrate. Hence, even using a 1.36 nm-thick aPHB nanolayer, we still did not observe as prominent a red shift of the carbonyl stretching band as was reported by Brogly et al. (a 10 cm⁻¹ shift) and Ulrent al. (a 8 cm⁻¹ shift). Therefore, this finding enables us to conclude that it is possible that the H-bonding interaction does not exist, or if it does, the interaction might be too subtle to be detected by the IRRAS measurement. In addition, molecular structural differences between PHB/PHBHx and PMMA may also be another reason for the absence of a H-bonding interaction. PHB/PHBHx has ester groups in the backbone, which is different from PMMA and EBA, where ester groups were located at the side chain. Side chain ester groups may result in a more effective contact of $-C \square O$ with an AO surface to form H-bonds. However, because the crystallization retardation effect is significant, we can conclude that apart from Hbonding interactions, there must be other molecular

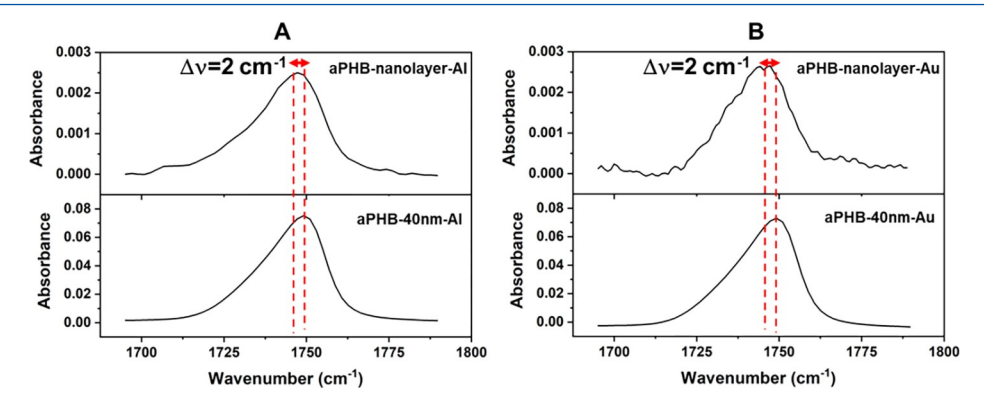


Figure 7. Comparison of IR carbonyl stretching region of aPHB nanolayer vs 40 nm layer on aluminum substrate (A) and gold substrate (B).

7348

interactions present, which contribute to this crystallization retardation phenomenon.

Dipole—Dipole Interaction between PHB/PHBHx and AO Surface. Though no H-bonding was detected, an interaction force such as a dipole—dipole interaction between an ester group and the AO surface may also play a critical role. We examined the surface energy of the two substrates. The relative polarity of each surface can be evaluated using an Owens and Wendt analysis.³⁹ The Owens and Wendt equation has the form of

is the form of
$$\mathbf{i}$$
 $\gamma l^{\mathrm{d}} \mathbf{y}$ \mathbf{j} $\gamma l^{\mathrm{p}} \mathbf{y}$ \mathbf{z} \mathbf{z}

where θ is the measured contact angle of a test liquid on the substrate, $\mathbf{Y}s^d$ and $\mathbf{Y}s^p$ are the dispersion component and the polar component of surface energy of the solid substrate, respectively, $\mathbf{Y}l^d$ and $\mathbf{Y}l^p$ are the dispersion component and the polar component of the test liquid, respectively. $\mathbf{Y}lv$ is the surface-free energy of the test liquid droplet under equilibrium with its vapor phase. The test liquids used are water and MI. The measured static contact angles are shown in Figure 8. The

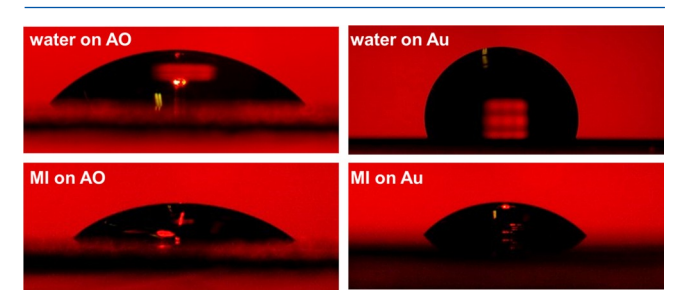


Figure 8. Measured static contact angles of water and MI on gold and AO surfaces.

derived surface-free energy terms for the two surfaces are listed in Table 2. It is observed that for gold, the dispersive force

Table 2. Calculated Surface Energy for Gold and Aluminum Substrates

surface	total surface energy (ergs/cm²)	polar component (ergs/cm²)	dispersion component (ergs/cm²)	polar contribution (%)
gold	44.71	0.53	44.18	1
AO	55.13	26.32	28.81	48

component dominates, whereas for AO, around 50% of the polar component contributes to the total surface energy. This finding indicates that AO has a highly polar surface. The crystallization of PHB and PHBHx relies on the intramolecular H-bonds formed between — To from one stem and — CH₃ groups from the neighboring stem. If— oinstead associates with O—Al—O from AO rather than associating with — CH₃ from the polymers, crystallization may be disrupted. In contrast, as shown in Table 2, the gold substrate has a dispersive surface, resulting in a weaker polymer/substrate interaction. Such a dispersive interaction is not expected to disrupt polymer crystallization.

However, we propose that dipole—dipole interactions may not be sufficient to result in such a prominent crystallization inhibition effect observed in the current study. In addition, another question that arises is why the AO surface promotes crystallization retardation but not a crystallization enhancement by serving as a nucleating template? We speculate that crystallization retardation or enhancement depends on the degree of order of the substrate surface. Figure 9 shows a high-

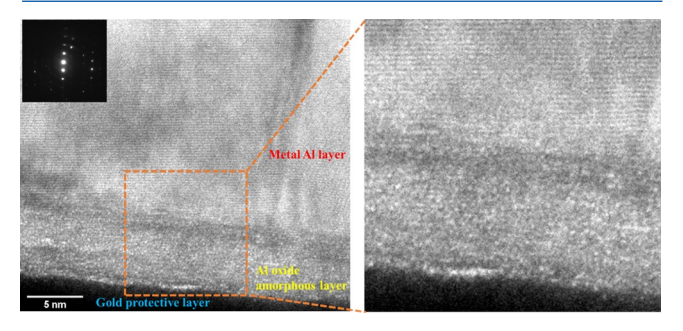


Figure 9. TEM high-resolution micrograph of Al/AO cross-sectional area. Left: overall view of the cross section and diffraction pattern from the metal layer. Right: a zoom-in to show clear lattice imaging.

resolution transmission electron microscopy (TEM) micrograph of an aluminum/AO interfacial region. One can clearly identify the bulk aluminum metal layer and its high crystallinity as indicated by the real-space lattice imaging and diffraction pattern. A 5 nm surface oxide layer was observed, which shows no lattice structure, indicating that it is disordered in nature. It is known that because of a required high activation energy, naturally formed metal oxide remains amorphous in the absence of an annealing treatment at high temperature.⁴⁰ The disordered AO surface will not facilitate polymer crystallization because of the absence of available crystalline facets to provide efficient nucleating sites. Instead, once the polymer is melted to form random coils, dipole-dipole interactions between the polymers and the disordered surface structure will anchor the polymer in a disordered state. The amorphous surface also provides nanoscale holes or sites to trap chain segments to prevent chain movement required for crystallization. The intrinsic stiffness and rigidity of a metal oxide surface will also inhibit chain relaxation. All these factors result even after cooling to room temperature (over 100 degree supercooling), indicating that the polymers can still exist in a supercooled amorphous state for an extended time period [over 12 h for PHBHx (13 mol %)], thereby contributing to the crystallization retardation phenomenon. Although the possibility of H-bond formation cannot be completely ruled out, our data indeed did not show a typical H-bond-induced red shift of the carbonyls. Thus, for a first approximation, we attribute the

the disordered nature of the AO surface.

Effect of the Aluminum Substrate on the Crystal Orientation. Crystal orientation profiles for the homopolymer PHB and the copolymer PHBHx (13 mol %) were investigated using GIWAXD on gold and aluminum substrates, as shown in Figure 10. All samples used for GIWAXD study were well crystallized at room temperature after 5 days. The appearance of the (020) reflection along the out-of-plane (perpendicular) direction indicates an edge-on lamellae orientation, whereas (20) appearing along the in-plane (horizontal) direction indicates a flat-on lamellar orientation. When crystallizing on gold, the edge-on oriented crystals predominate, but a fair amount of flat-on oriented crystals can also be seen as indicated by a weak (020) reflection along the horizontal

crystallization retardation to the dipole-dipole interaction and

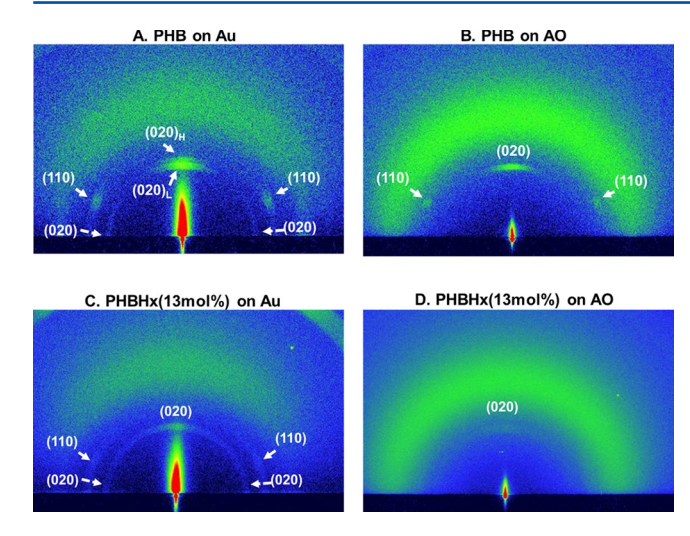


Figure 10. GIWAXD profiles for a PHB crystalline film on gold (A), PHB crystalline film on AO (B), PHBHx (13 mol %) film on gold (C), and PHBHx (13 mol %) film on AO (D).

direction. In addition, for PHB/Au, along the out-of-plane direction, we see a second (020) peak, denoted as (020)H, with a smaller d-spacing (higher reflection angle), suggesting a more perfect alpha crystal. It is most likely that these more perfect crystals were developed during the cooling step. This observation is consistent with the IRRAS data and the Avrami analysis. Two d-spacings of the (020) peak were also observed by Khasanah et al.⁴¹ In contrast, on an aluminum substrate, both PHB and PHBHx (13 mol %) show only edge-on orientation, and no flat-on orientation was observed. This substrate-induced crystal orientation difference will be discussed in a later section. In addition, based on the diffraction pattern observed on either on gold or aluminum, the overall reflection intensity for PHBHx (13 mol %) is much weaker than that of PHB because of its intrinsic lower crystallinity.

Proposed Mechanism for Edge-on Crystal Orientation of PHB/PHBHx on Aluminum Substrate. Now, a possible explanation for why the crystallites only show edge-on orientation, as indicated by the GIWAXD data in Figure 10, on aluminum substrates (or AO) will be discussed. Let us first examine the sample of PHBHx (13 mol %) on Au (Figure 10C) and AO (Figure 10D). Both samples have edge-on crystals as indicated by the (020) peak along the perpendicular direction, whereas PHBHx 13 (mol %) on Au also has flat-on crystals as indicated by the (020) peak along the horizontal direction. These two samples crystallize isothermally at room temperature; therefore, both have the same crystallization temperature profile. Thus, the orientation profile difference is not due to a temperature effect but possibly due to a substrate effect. Typically, a low crystallization temperature facilitates edge-on crystal formation, 42 and room temperature for PHBHx is a low crystallization temperature. Therefore, the flat-on crystals for PHBHx (13 mol %) on Au is most likely due to a confinement effect. It is well known that the confinement effect can induce a flat-on crystal orientation.³¹ In our case, the flaton crystals were most likely developed in the confinement layer of the polymer/Au substrate interface, where the polymer is confined by the bottom substrate. Such confinement-induced flat-on crystals for PHB have been studied extensively by Khasanah et al.⁴¹ In their work, it has been found that PHB in the confinement layer tends to form flat-on crystals, whereas

polymers near the film surface (polymer/air interface) tend to crystallize into edge-on crystals. The proposed hypothesis for the absence of confinement-induced flat-on crystals for PHBHx (13 mol %) on AO is shown below in Figure 11.

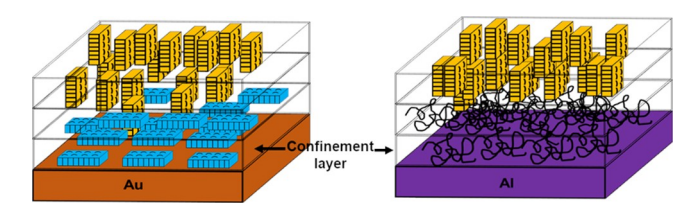


Figure 11. Simplified schematic to illustrate crystal orientation profiles in PHB and PHBHx (13 mol %) ultrathin films on gold (left) and aluminum (right). Edge-on crystal (yellow) and flat-on crystal (blue).

On AO, because of a crystallization inhibition effect, the formation of flat-on crystals in the confinement layer is significantly inhibited. In contrast, polymers on the film surface can still crystallize to adopt an edge-on orientation. These early developed edge-on crystals may even induce the confinement layer to adopt the same edge-on orientation, resulting in an edge-on dominated crystal orientation throughout the entire film, as shown in Figure 11. Now, let us examine PHB on AO (Figure 10B), which was also isothermally crystallized at room temperature. The exclusive edge-on orientation for PHB on AO is believed to be similar to that for PHBHx (13 mol %) on AO, that is, the flat-on crystals in the confinement layer that normally form were inhibited because of the crystallization inhibition effect of AO. For PHB on Au (Figure 10A), the flaton crystals may be caused by a similar confinement-induced flat-on orientation as observed for the case of PHBHx (13 mol %) on Au. A second possibility involves a high-temperatureinduced flat-on orientation. Because PHB crystallizes quickly on Au, although the majority of the crystallization occurs after cooling to room temperature, crystallization may have already begun during the cooling process. This is supported by observation of a weak intensity peak at 1230 cm⁻¹ in the 2 min IRRAS spectrum shown in Figure 1. It is known that a high crystallization temperature typically facilitates flat-on lamellar orientation. 42 Thus, part of the flat-on crystals may originate from high-temperature crystallization.

The scientific insights gained from the current study lie in the following points: (1) our results partially answered the question raised by Napolitano and Wübbenhorst²E"in PHB ultrathin films sandwiched between two aluminum plates, is the crystallization retardation due to a confinement effect or the intrinsic AO surface chemistry effect?". Our work clearly showed that the intrinsic chemistry and the disordered structure of the AO surface can cause a significant crystallization retardation effect; (2) it would not be surprising to observe such a crystallization retardation effect if the polymer interacts with the AO surface via strong interactions such as chemical bonds or strong H-bonds. In our case, however, all the evidence points toward a van der Waals interaction (the dipole-dipole interaction for PHB/AO), a conventionally weak interaction, together with a disordered surface that can give rise to such a prominent crystallization retardation; and (3) because of the wide use of metal oxide materials in the polymer processing industry, it would be important to extend the current study to other metal oxides and other polymers containing polar functional groups in a

more systematic investigation. Our results will provide more insights into the design of substrate surfaces so as to tune the structure and properties of thin films of semicrystalline polymers.

CONCLUSIONS

In this study, we discovered that an AO flat surface was able to retard the overall crystallization rate of the homopolymer PHB and random copolymers PHBHx thin films. Because of the free nature of one side of the film, the spatial confinement was only located in the confinement layer near the region of polymer/ substrate interface, suggesting that the retardation effect purely originated from an AO surface interaction with the polymers. By performing Avrami analysis on the kinetic profiles, we found that the crystallization rate constant $k \, (\min^{-1})$ for all the polymers on AO is approximately 3 to 4 orders of magnitude less than that found for the same polymers on gold. No Hbond formation between the studied polyesters and an AO surface hydroxyl was detected, as indicated by no substantial red shift of the carbonyl frequency found for nanolayer aPHB on AO. However, the possibility of weak H-bonding association cannot be completely excluded. Surface energy profile analysis indicated that AO has a polar surface, which can interact with PHB/PHBHx through dipole-dipole interactions. A rigid, disordered surface of AO was proposed as another critical factor to retard crystallization, and we concluded that the retardation effect mainly originates from the sum of dipole-dipole interactions between the polymer and the disordered nature of AO surface. Both flat-on and edge-on orientated crystallites on gold were observed, whereas on AO, only edge-on oriented crystallite orientation were found. This unique edge-on orientation for PHB/PHBHx on AO is most likely due to crystallization of polymers in the confinement region where flat-on crystals are inhibited due to the polymer/substrate interaction.

ASSOCIATED CONTENT

Supporting Information

The Supporting Information is available free of charge on the ACS Publications website at DOI: 10.1021/acs.macromol.9b01214.

Surface topographies of aluminum and gold substrates; typical XRR profile for spin-coated PHB/PHBHx ultrathin films; experimental details for the melting of each sample; XPS survey spectrum; schematic plot of "S"-shaped crystallization kinetics profile; magnified backbone region of IR spectra for PHB on Au and Al substrates; and preparation conditions and thickness calculation for a PHB nanolayer (PDF)



AUTHOR INFORMATION

Corresponding Author

*E-mail: rabolt@udel.edu.

ORCID ®

Changhao Liu: 0000-0002-9103-8834 Meng Jia: 0000-0002-8586-2384 John F. Rabolt: 0000-0003-4132-4266

Notes

The authors declare no competing financial interest.

ACKNOWLEDGMENTS

This publication was made possible by the National Science Foundation (NSF) EPSCoR grant nos. 1301765 and 1757353 and the State of Delaware. The authors would like to acknowledge the support from the NSF DMR Polymers Program Grant DMR 1407255. The authors also acknowledge the funding of NSF 1428149 for Thermo Scientific K-Alpha instruments. Prof. Lars Gundlach is acknowledged for his support of M.J.'s work on the project.

REFERENCES

- (1) Philip, S.; Keshavarz, T.; Roy, I. Polyhydroxyalkanoates: Biodegradable Polymers with a Range of Applications. *J. Chem. Technol. Biotechnol.* 2007, 82, 233–247.
- (2) Noda, I.; Green, P. R.; Satkowski, M. M.; Schechtman, L. A. Preparation and Properties of a Novel Class of Polyhydroxyalkanoate Copolymers. *Biomacromolecules* 2005, *6*, 580–586.
- (3) Noda, I.; Lindsey, S. B.; Caraway, D. NodaxTM Class PHA Copolymers: Their Properties and Applications. In *Plastics from Bacteria: Natural Functions and Applications*; Chen, G. G.-Q., Ed.; Microbiology Monographs; Springer Berlin Heidelberg: Berlin, Heidelberg, 2010; pp 237–255.
- (4) Anderson, A. J.; Dawes, E. A. Occurrence, Metabolism, Metabolic Role, and Industrial Uses of Bacterial Polyhydroxyalkanoates. *Microbiol. Rev.* 1990, 54, 450.
- (5) Philip, S.; Keshavarz, T.; Roy, I. Polyhydroxyalkanoates: Biodegradable Polymers with a Range of Applications. *J. Chem. Technol. Biotechnol.* 2007, 82, 233–247.
- (6) Yokouchi, M.; Chatani, Y.; Tadokoro, H.; Teranishi, K.; Tani, H. Structural Studies of Polyesters: 5. Molecular and Crystal Structures of Optically Active and Racemic Poly (β-Hydroxybutyrate). *Polymer* 1973, 14, 267–272.
- (7) Wang, H.; Tashiro, K. Reinvestigation of Crystal Structure and Intermolecular Interactions of Biodegradable Poly(3-Hydroxybutyrate) α-Form and the Prediction of Its Mechanical Property. *Macromolecules* 2016, 49, 581–594.
- (8) Iwata, T.; Fujita, M.; Aoyagi, Y.; Doi, Y.; Fujisawa, T. Time-Resolved X-Ray Diffraction Study on Poly[(R)-3-Hydroxybutyrate] Films during Two-Step-Drawing: Generation Mechanism of Planar Zigzag Structure. *Biomacromolecules* 2005, *6*, 1803–1809.
- (9) Iwata, T.; Aoyagi, Y.; Tanaka, T.; Fujita, M.; Takeuchi, A.; Suzuki, Y.; Uesugi, K. Microbeam X-Ray Diffraction and Enzymatic Degradation of Poly[(R)-3-Hydroxybutyrate] Fibers with Two Kinds of Molecular Conformations. *Macromolecules* 2006, 39, 5789–5795.
- (10) Orts, W. J.; Marchessault, R. H.; Bluhm, T. L.; Hamer, G. K. Observation of Strain-Induced β Form in Poly(β-Hydroxyalkanoates). *Macromolecules* 1990, 23, 5368–5370.
- (11) Liu, C.; Noda, I.; Martin, D. C.; Chase, D. B.; Ni, C.; Rabolt, J. F. Growth of Anisotropic Single Crystals of a Random Copolymer, Poly[(R)-3-Hydroxybutyrate-Co-(R)-3-Hydroxybexanoate] Driven by Cooperative CH ··· O H-Bonding. *Polymer* 2018, 154, 111—118.
- (12) Sato, H.; Mori, K.; Murakami, R.; Ando, Y.; Takahashi, I.; Zhang, J.; Terauchi, H.; Hirose, F.; Senda, K.; Tashiro, K.; et al. Crystal and Lamella Structure and C—H···OC Hydrogen Bonding of Poly(3-Hydroxyalkanoate) Studied by X-Ray Diffraction and Infrared Spectroscopy. *Macromolecules* 2006, 39, 1525–1531.
- (13) Sato, H.; Murakami, R.; Padermshoke, A.; Hirose, F.; Senda, K.; Noda, I.; Ozaki, Y. Infrared Spectroscopy Studies of CH···O Hydrogen Bondings and Thermal Behavior of Biodegradable Poly(Hydroxyalkanoate). *Macromolecules* 2004, 37, 7203–7213.
- (14) Sato, H.; Ando, Y.; Dybal, J.; Iwata, T.; Noda, I.; Ozaki, Y. Crystal Structures, Thermal Behaviors, and C-H···O=C Hydrogen Bondings of Poly(3-Hydroxyvalerate) and Poly(3-Hydroxybutyrate) Studied by Infrared Spectroscopy and X-Ray Diffraction. *Macromolecules* 2008, 41, 4305–4312.
- (15) Tanaka, T.; Yabe, T.; Teramachi, S.; Iwata, T. Mechanical Properties and Enzymatic Degradation of Poly[(R)-3-Hydroxybuty-

rate] Fibers Stretched after Isothermal Crystallization near Tg. *Polym. Degrad. Stab.* 2007, 92, 1016–1024.

- (16) Aoyagi, Y.; Doi, Y.; Iwata, T. Mechanical Properties and Highly Ordered Structure of Ultra-High-Molecular-Weight Poly[(R)-3-Hydroxybutyrate] Films: Effects of Annealing and Two-Step Drawing. *Polym. Degrad. Stab.* 2003, 79, 209–216.
- (17) Fukada, E.; Ando, Y. Piezoelectric Properties of Poly-β-Hydroxybutyrate and Copolymers of β-Hydroxybutyrate and β-Hydroxyvalerate. *Int. I. Biol. Macromol.* 1986, 8, 361–366.
- (18) Horowitz, D. M.; Sanders, J. K. M. Amorphous, Biomimetic Granules of Polyhydroxybutyrate: Preparation, Characterization, and Biological Implications. *J. Am. Chem. Soc.* 1994, 116, 2695–2702.
- (19) de Koning, G. J. M.; Lemstra, P. J. The Amorphous State of Bacterial Poly[(R)-3-Hydroxyalkanoate]in Vivo. *Polymer* 1992, 33, 3292–3294
- (20) Dai, X.; Li, H.; Ren, Z.; Russell, T. P.; Yan, S.; Sun, X. Confinement Effects on the Crystallization of Poly(3-Hydroxybuty-rate). *Macromolecules* 2018, *51*, 5732–5741.
- (21) Dai, X.; Zhang, J.; Ren, Z.; Li, H.; Sun, X.; Yan, S. A Grazing Incident XRD Study on the Structure of Poly(3-Hydroxybutyrate) Ultrathin Films Sandwiched between Si Wafers and Amorphous Polymers. *Polym. Chem.* 2016, 7, 3705–3713.
- (22) Napolitano, S.; Wubbenhorst, M. Slowing Down of the Crystallization Kinetics in Ultrathin Polymer Films: A Size or an Interface Effect? *Macromolecules* 2006, 39, 5967–5970.
- (23) Capitan M. J.; Rueda, D. R.; Ezquerra, T. A. Inhibition of the Crystallization in Nanofilms of Poly(3-Hydroxybutyrate). *Macromolecules* 2004, 37, 5653–5659.
- (24) Greenler, R. G. Infrared Study of Adsorbed Molecules on Metal Surfaces by Reflection Techniques. J. Chem. Phys. 1966, 44, 310–315. (25) Moulder, J. F. Handbook of X-Ray Photoelectron Spectroscopy;

Physical Electronics Division, 1995; pp 230-232.

- (26) Yu, J.; Asai, S.; Sumita, M. Time-Resolved FTIR Study of Crystallization Behavior of Melt-Crystallized Poly(Phenylene Sulfide). *I. Macromol. Sci., Part B: Phys.* 2000, 39, 279–296.
- (27) Chen, L.; Yu, Z.-W. Crystallization Behavior of DSPE in Dimethyl Sulfoxide by Time-Resolved Infrared Spectroscopy and Differential Scanning Calorimetry. *J. Macromol. Sci., Part B: Phys.* 2002 41 137–147
- (28) Chen, Y.; Park, Y.; Noda, I.; Jung, Y. M. Influence of Polyethylene Glycol (PEG) Chain Length on the Thermal Behavior of Spin-Coated Thin Films of Biodegradable Poly(3-Hydroxybutyrate-Co-3-Hydroxyhexanoate)/PEG Blends. *J. Mol. Struct.* 2016, 1124, 159–163.
- (29) Chen, Y.; Noda, I.; Jung, Y. M. Revealing Thermal Behavior of Poly(3-Hydroxybutyrate-Co-3-Hydroxyhexanoate) and Its Polyethylene Glycol Blends Thin Films: Effect of 3-Hydroxyhexanoate Comonomer Content. *I. Mol. Struct.* 2018, *1162*, 140–144.
- (30) Noda, I.; Dowrey, A. E.; Haynes, J. L.; Marcott, C. Group Frequency Assignments for Major Infrared Bands Observed in Common Synthetic Polymers. In *Physical Properties of Polymers Handbook*; Mark, J. E., Ed.; Springer New York: New York, NY, 2007; pp. 395–406.
- (31) Wang, H.; Keum, J. K.; Hiltner, A.; Baer, E.; Freeman, B.; Rozanski, A.; Galeski, A. Confined Crystallization of Polyethylene Oxide in Nanolayer Assemblies. *Science* 2009, 323, 757–760.
- (32) Wang, H.; Keum, J. K.; Hiltner, A.; Baer, E. Crystallization Kinetics of Poly(Ethylene Oxide) in Confined Nanolayers. *Macromolecules* 2010, 43, 3359–3364.
- (33) Ponting, M.; Lin, Y.; Keum, J. K.; Hiltner, A.; Baer, E. Effect of Substrate on the Isothermal Crystallization Kinetics of Confined Poly(ε-Caprolactone) Nanolayers. *Macromolecules* 2010, 43, 8619–8627.
- (34) Avrami, M. Kinetics of Phase Change. I General Theory. J. Chem. Phys. 1939, 7, 1103–1112.
- (35) Choi, H. W.; Kim, Y. H.; Rim, Y. H.; Yang, Y. S. Crystallization Kinetics of Lithium Niobate Glass: Determination of the Johnson—Mehl—Avrami—Kolmogorov Parameters. *Phys. Chem. Chem. Phys.* 2013, *15*, 9940.

(36) An, Y.; Dong, L.; Mo, Z.; Liu, T.; Feng, Z. Nonisothermal Crystallization Kinetics of Poly(β-Hydroxybutyrate). *J. Polym. Sci., Part B: Polym. Phys.* 1998, 36, 1305–1312.

- (37) Brogly, M.; Grohens, Y.; Labbe, C.; Schultz, J. Influence of Tacticity on the Conformation and Development of Acid-Base Adducts of PMMA Homopolymers Adsorbed on Aluminium Mirrors. *Int. J. Adhes. Adhes.*, 1997, 17, 257–261.
- (38) Ulren L.; Hjertberg, T.; Ishida, H. An FT-IR Study on Interfacial Interactions in Ethylene Copolymers/Aluminium Laminates in Relation to Adhesion Properties. *J. Adhes.* 1990, 31, 117–136.
- (39) Owens, D. K.; Wendt, R. C. Estimation of the Surface Free Energy of Polymers. *J. Appl. Polym. Sci.* 1969, 13, 1741–1747.
- (40) Jeurgens, L. P. H.; Śloof, W. G.; Tichelaar, F. D.; Mittemeijer, E. J. Structure and Morphology of Aluminium-Oxide Films Formed by Thermal Oxidation of Aluminium. *Thin Solid Films* 2002, 418, 89–101
- (41) Khasanah; Reddy, K. R.; Ogawa, S.; Sato, H.; Takahashi, I.; Ozaki, Y. Evolution of Intermediate and Highly Ordered Crystalline States under Spatial Confinement in Poly(3-Hydroxybutyrate) Ultrathin Films. *Macromolecules* 2016, 49, 4202–4210.
- (42) Sun, X.; Gao, N.; Li, Q.; Zhang, J.; Yang, X.; Ren, Z.; Yan, S. Crystal Morphology of Poly(3-Hydroxybutyrate) on Amorphous Poly(Vinylphenol) Substrate. *Langmuir* 2016, 32, 3983–3994.